NJC

ROYAL SOCIETY OF CHEMISTRY

PAPER

View Article Online
View Journal

Cite this: DOI: 10.1039/d0nj04434b

A stable, highly oxidizing radical cation†

N. Harsha Attanayake, Aman Preet Kaur, T. Malsha Suduwella, Corrine F. Elliott, Sean R. Parkin and Susan A. Odom *

Received 10th September 2020,
Accepted 7th October 2020

DOI: 10.1039/d0nj04434b

rsc.li/njc

Highly oxidizing radical cation salts can be used as chemical oxidants in a wide variety of applications. While some are commercial and others can be made, stability has been a problem with many of these organic-based reagents. We sought a method to increase redox potentials of organic compounds, to yield radical cation salts that do not suffer the same instability as their triarylamine counterparts. Using phenothiazines, we (i) blocked the positions *para* to nitrogen with a substituent containing strong covalent bonds, using an electron-withdrawing group to increase oxidation potential, while at the same time (ii) introduced strain at the positions *ortho* to nitrogen to further raise the oxidation potential by preventing geometric relaxation of the oxidized state. Here we synthesized the phenothiazine derivative, *N*-ethyl-1,9-dimethyl-3,7-bis(trifluoromethyl)phenothiazine to test this hypothesis. Indeed, oxidation potentials reflect additive substituent effects, yielding a high-potential redox couple with a stable radical cation. Stability tests in solution and the solid state show that the radical cation form of this phenothiazinium is stable and can be used to oxidize other organic compounds in solution.

Introduction

The introduction of substituents on a redox-active core is a common method used to tailor oxidation and reduction potentials.[1–3] The degree of change *vs.* an original core can often be reliably predicted using Hammett constants, which quantify the degree of electron donation or withdrawal.[3,4] A desire to create high oxidation potential redox couples for electronic and energetic applications has resulted in the synthesis of new materials that contain strongly electron-withdrawing groups.[1,5] For example, in developing redox mediators for applications in electrochemical energy storage, our group and others have reported dialkoxybenzene,[5–8] TEMPO,[9–11] phenothiazine,[12–14] and triarylamine derivatives[15–17] that contain electron-withdrawing groups as high potential materials for overcharge protection in lithium-ion batteries (LIBs), posolytes for redox flow batteries, and redox mediators for lithium–air batteries.

While the incorporation of electron-withdrawing groups can be used to reach high oxidation potentials, problems in stability can arise if these redox couples are employed in reducing environments.[5,18] Otherwise stable redox couples often decompose if reduced to their radical anion forms.[18,19] For example, dialkoxybenzenes containing phosphonate substituents with oxidation potentials higher than 4 V *vs.* $Li^{0/+}$ (this corresponds to about 0.8 V *vs.* ferrocene/ferrocenium) were designed for overcharge protection of LIBs containing high voltage cathodes. Compared to their lower potential counterparts, their lifetimes in this application were dramatically reduced when employed in electrochemical cells containing highly reducing graphitic anodes.[19,20] However, in some cases, less reducing lithium titanate anodes resulted in prolonged lifetimes.[21] We suspected that reduction to the radical anion form in graphitic anode-containing cells was the cause of the limited lifetimes. Cyclic voltammetry of these derivatives shows that irreversible reduction events are accessible in the electrolyte window, whereas without the electron-withdrawing groups, reduction events were too low in potential to be observed. Our group has observed similar results in the development of high-potential phenothiazine derivatives that oxidize at or above 4 V *vs.* $Li^{0/+}$ (*ca.* 0.8 V *vs.* $Cp_2Fe^{0/+}$).[1,18] Clearly, a different strategy must be employed for the development of high potential redox couples that exhibit reductive stability.

Apart from the applications in energy storage, the charged forms of stable, high-potential materials are of interest as initiators and as chemical oxidants in organic synthesis.[22,23] The electron-donating, high oxidation potential organic compounds with stable charged states are interesting as organic photoredox catalysts (as powerful oxidants) to perform reductive electron-transfer reactions.[24,25] However, most of the radical cations have very short lifetime in solution phase, which characteristic we attribute to their low-lying excited state energies.[25–28] The short lifetimes prevent utilizing radical cations as powerful oxidants.[25] Thus, developing organic materials with

Department of Chemistry, University of Kentucky, Lexington, KY 40506, USA. E-mail: susan.odom@uky.edu

† Electronic supplementary information (ESI) available. CCDC 1589385, 2006455–2006457. For ESI and crystallographic data in CIF or other electronic format see DOI: 10.1039/d0nj04434b

stable charged forms is needed for the growth of the field of metal-free photoredox chemistry. Also, to be useful as a chemical oxidant, the neutral form of the aromatic compound should have a high oxidation potential and its charged species (radical cation) should have a high chemical stability in the solid phase (for storage purposes) as well as in solution phase (to perform redox reactions).[29–31]

An alternative method to modulating redox potentials is to vary conjugation in electronic materials.[32,33] This approach has been employed by altering dihedral angles between conjugated pi systems, such as polyphenylenes and polythiophenes, as well as twisting or bending a planar pi system, such as in twistacenes and fullerenes.[34–36] Often these changes are designed in neutral forms of the redox cores and are retained in their oxidized or reduced states. Recently, we found that a new approach could be used to tune oxidation potentials in a class of molecules called phenothiazines.[37] These heterocyclic fused-ring systems exhibit a bent geometry in their neutral form, and planarize upon oxidation. We found that preventing planarization of the oxidized form, without significantly altering the molecular geometry of the neutral form, resulted in an increase in oxidation potential, offering a route to high potential couples without requiring electron-withdrawing groups.[37] In fact, even the use of electron-donating methyl groups, which usually lower oxidation potentials of conjugated molecules, raises the oxidation potentials of phenothiazines if placed appropriately.

Compared to a parent compound, *N*-ethylphenothiazine (EPT, Fig. 1), a derivative containing methyl groups *para* to nitrogen, *N*-ethyl-3,7-dimethylphenothiazine (3,7-DMeEPT, Fig. 1) has a lower oxidation potential, which is expected based on the electron-donating nature of methyl substituents. However, when the methyl groups are placed *ortho* to nitrogen, as with *N*-ethyl-1,9-dimethylphenothiazine (1,9-DMeEPT, Fig. 1), the effect on oxidation potential is not only the opposite but is larger in magnitude. The impact is nearly as significant as the introduction of two trifluoromethyl groups *para* to nitrogen, as with *N*-ethyl-3,7-bis(trifluoromethyl)phenothiazine (3,7-BCF$_3$EPT, Fig. 1). Oxidation potentials are provided in Table 1.

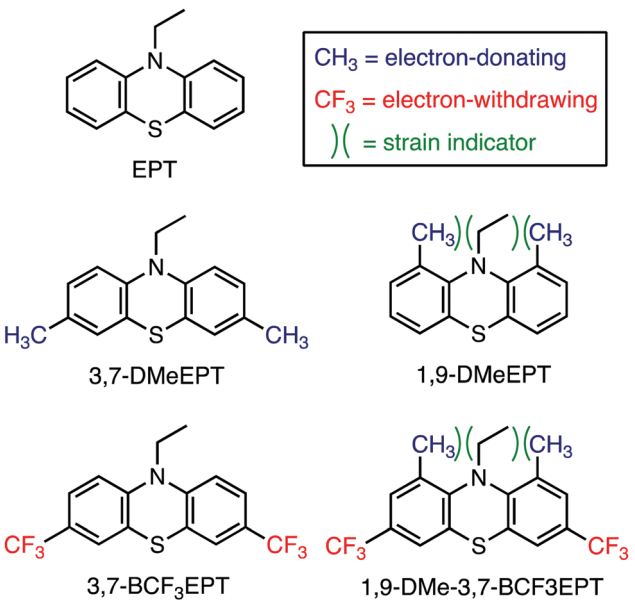

Fig. 1 Representations of the chemical structures of *N*-ethylphenothiazine (EPT), *N*-ethyl-3,7-dimethylphenothiazine (3,7-DMeEPT), *N*-ethyl-1,9-dimethylphenothiazine (1,9-DMeEPT), *N*-ethyl-3,7-bis(trifluoromethyl)phenothiazine (3,7-BCF$_3$EPT), and *N*-ethyl-1,9-dimethyl-3,7-bis(trifluoromethyl)phenothiazine (1,9-DMe-3,7-BCF$_3$EPT).

Table 1 Comparison of butterfly angles of neutral and radical cation forms of phenothiazine derivatives, obtained from X-ray crystallography. The radical cations salts had hexachloroantimonate ($SbCl_6^-$) as the counter ion. Half-wave first oxidation potentials ($E_{1/2}^{0/+}$) *vs.* $Cp_2Fe^{0/+}$

Compound	Butterfly angles [°]		$E_{1/2}^{0/+}$ *vs.* $Cp_2Fe^{0/+}$ (V)
	Neutral	Radical cation	
EPT	136.8[a]	174.8[a]	0.27
3,7-DMeEPT	149.3[a]	174.9	0.13
1,9-DMeEPT	146.5[a]	164.9	0.53
3,7-BCF$_3$EPT	144.5–152.1[ab]	164.5[ab]	0.61
1,9-DMe-3,7-BCF$_3$EPT	140.5	162.8	0.88

[a] Ref. 37 [b] Multiple molecules in asymmetric unit.

Seeking even higher redox potentials, we wondered whether the effects of electron-withdrawing groups (as in 3,7-BCF$_3$EPT)[38] and sterically hindering groups (as in 1,9-DMeEPT)[37] could be combined constructively to achieve this goal. It was unclear, for example, if the electron-withdrawing effect of the trifluoromethyl groups would be disrupted by the sterically hindering groups preventing relaxation, or would the effect be combined? To answer this question, we targeted a new compound, *N*-ethyl-1,9-dimethyl-3,7-bis(trifluoromethyl)phenothiazine (1,9-DMe-3,7-BCF$_3$EPT, Fig. 1), incorporating methyl groups at the *ortho* positions for the steric effect and trifluoromethyl groups at the *para* positions to harness their electron-withdrawing effect. Here we report the synthesis and characterization of this new derivative in comparison to the related compounds shown in Fig. 1, and demonstrate its use as a shelf-stable chemical oxidant.

Results and discussion

The synthesis of 1,9-DMe-3,7-BCF$_3$EPT (Scheme 1) was accomplished in three steps starting from 1,9-DMePT, which was synthesized following a previously reported procedure for the same compound.[37] Bromination of 1,9-DMePT produced intermediate 1,9-DMe-3,7-DBrPT, which was then alkylated to obtain 1,9-DMe-3,7-DBrEPT. Finally, 1,9-DMe-3,7-BCF$_3$EPT was synthesized by treating 1,9-DMe-3,7-DBrEPT with a combination of potassium trifluoroacetate, copper(I) iodide, and cesium fluoride. Synthetic procedures and characterization information are reported in the Experimental section.

In addition to standard spectroscopic techniques, X-ray diffraction of single-crystals of 1,9-DMe-3,7-BCF$_3$EPT (Fig. 2) provide further support of this product's identity. The thermal ellipsoid plot shows that this derivative is bent through the *N* and *S* atoms, with a butterfly angle (the angle formed by the

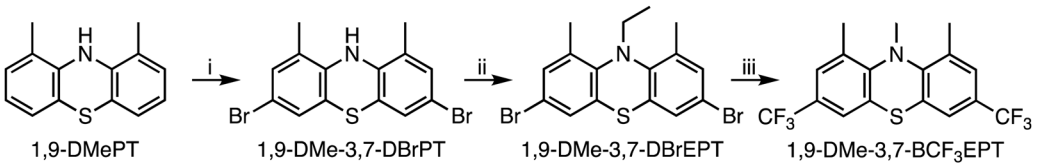

Scheme 1 Synthetic route used to obtain 1,9-DMe-3,7-BCF_3EPT. i. Br_2, CH_3COOH, 24-36 h, r.t. (2.78 g, 51%), ii. (a). NaH, DMF/THF, r.t., 30 min, (b). CH_3CH_2Br, 80 °C, o/n, (2.15 g, 66%), iii. CF_3CO_2K, CuI, CsF, NMP/DMI, 180 °C, 48 h (0.62 g, 48%).

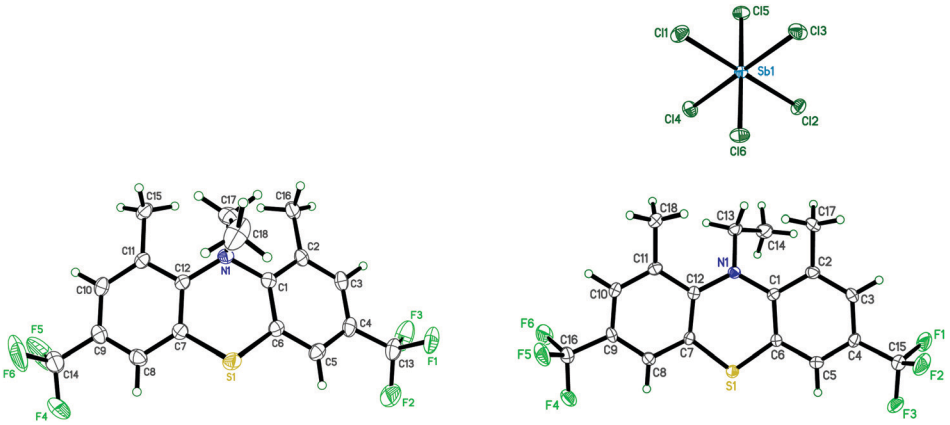

Fig. 2 Thermal ellipsoid plot of neutral (left) and radical cation (right) of 1,9-DMe-3,7-BCF_3EPT, obtained by single-crystal X-ray diffraction. The radical cation salts have hexachloroantimonate ($SbCl_6^-$) as the counter ion.

intersection of the phenyl-ring planes) of 140.5°. This angle is nearly identical to that of 1,9-DMeEPT (146.5°), which does not deviate significantly from derivatives containing *para* substituents, 3,7-DMeEPT (149.3°), and 3,7-BCF_3EPT (144.5–152.1°). All compounds are less bent than the unsubstituted parent EPT (136.8°), (Table 1 and Fig. S1, ESI†). The main difference in geometries of the 1,9-dimethylated derivatives is expected to be in their radical cation forms. To compare the geometries of radical cations with their neutral forms, we synthesized and isolated the radical cation salts of all EPT derivatives through chemical oxidation with antimony pentachloride ($SbCl_5$). The radical cation salts had hexachloroantimonate ($SbCl_6^-$) as the counter ion. To confirm identity, we grew crystals of radical cation salts and conducted analysis using X-ray diffraction. The thermal ellipsoid plots of radical cation salts are shown in Fig. 2 and Fig. S1 (ESI†). In addition, we compared butterfly angles in these systems to results from density functional theory (DFT), as we know they are a reliable predictor of molecular geometries in this class of molecules. DFT calculations predict the radical cation butterfly angle for 1,9-DMe-3,7-BCF_3EPT to be 156.9°, which is similar to the computed value for the radical cation of 1,9-DMeEPT (156.6°). The isolated single-crystals of 1,9-DMe-3,7-BCF_3EPT and 1,9-DMeEPT radical cations show butterfly angles of 162.8° and 164.9° respectively, confirming that charged forms of strained phenothiazines remain bent. By contrast, the calculated butterfly angles of the radical cations of unstrained derivatives EPT, 3,7-DMeEPT, and 3,7-BCF_3EPT are significantly more planar; all lie between 171 and 172°, which are close to experimentally obtained values (174° to 175°). These results suggest that, like 1,9-DMeEPT, the geometric relaxation of the radical cation of 1,9-DMe-3,7-BCF_3EPT will be limited. The experimental and calculated butterfly angles are given in Table 1 and Table S2 (ESI†), respectively. The calculated adiabatic ionization potential (AIP) of 1,9-DMe-3,7-BCF_3EPT is consistent with this trend (Fig. 3 and Table S1, ESI†). In fact, the AIP for 1,9-DMe-3,7-BCF_3EPT (7.22 eV, +0.74 eV *vs.* EPT at 6.48 eV) is almost the sum of the effect of the substituents on their simpler counterparts, 1,9-DMeEPT (6.68 eV, +0.20 eV *vs.* EPT) and 3,7-BCF_3EPT (7.06 eV, +0.58 eV *vs.* EPT). See Table S1 (ESI†) for AIP values.

Cyclic voltammetry (CV) was performed to determine the half-wave oxidation potential and chemical reversibility of 1,9-DMe-3,7-BCF_3EPT. This experiment was done in 0.1 M tetrabutylammonium hexafluorophosphate (n-Bu_4NPF_6) in DCM. A cyclic voltammogram of 1,9-DMe-3,7-BCF_3EPT is shown in Fig. 4a. It shows a first reversible oxidation and a second irreversible oxidation (Fig. S4, ESI†). No reduction event was observed. The first oxidation, at 0.88 V *vs.* $Cp_2Fe^{0/+}$ at 0 V, is the highest in the series of compounds studied. Compared to EPT ($E_{1/2}^{0/+}$ = 0.27 V *vs.* $Cp_2Fe^{0/+}$), the oxidation potential of 1,9-DMeEPT ($E_{1/2}^{0/+}$ = 0.53 V *vs.* $Cp_2Fe^{0/+}$) is 0.26 V higher, and that of 3,7-BCF_3EPT ($E_{1/2}^{0/+}$ = 0.61 V *vs.* $Cp_2Fe^{0/+}$) is 0.34 V higher. The oxidation potential of 1,9-DMe-3,7-BCF_3EPT is nearly identical to what would be predicted by simply combining the effects of the *ortho* methyl substituents and *para* trifluoromethyl substituents (0.87 V *vs.* $Cp_2Fe^{0/+}$), supporting the proposition that the

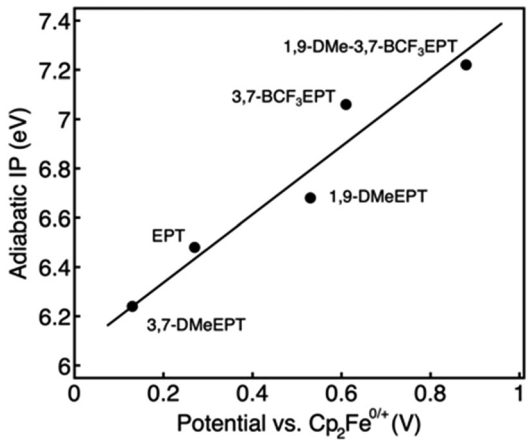

Fig. 3 Plot of calculated AIPs *vs.* half-wave oxidation potentials. The equation for the line of best fit, $y = 0.7039x - 4.257$, has an R^2 value of 0.94.

effect of the substituents is indeed additive. These values are in good agreement with the calculated AIPs, as shown in a plot of AIP *vs.* $E^{0/+}_{1/2}$ (Fig. 3), for which a line of best fit has an R^2 value of 0.94.

The first oxidation is chemically reversible in this electrolyte, as evidenced by the ratio of forward to reverse current (I_{pa}/I_{pc}) of 1.05 (Table S1, ESI†). Variable scan rate voltammograms (Fig. 4b and Fig. S5, ESI†) were performed to determine values of the diffusion coefficients of the neutral and radical cations, determined from Randles–Sevcik plots (Fig. 4c and Fig. S5, ESI†). The diffusion coefficient for neutral 3,7-DMeEPT, 3,7-BCF_3EPT, and 1,9-DMe-3,7-BCF_3EPT are nearly the same, and are all slower than derivatives without *para* substituents. However, the case of the radical cations is more variable, with rates increasing as follows: 1,9-DMe-3,7-BCF_3EPT < 3,7-DMeEPT < 3,7-BCF_3EPT < 1,9-DMeEPT < EPT. While the derivatives without *para* substituents again have the highest diffusion coefficients, the substituent positions are not enough to explain the trend. Perhaps two trends are competing, such as molecular shape and charge distribution, both of which could affect the solvation spheres.

Given that the first oxidation event was reversible on the CV time scale, at scan rates as low as 25 mV s^{-1}, we wanted to further evaluate the stability of the radical cation form of 1,9-DMe-3,7-BCF_3EPT, as radical cations are generally the more reactive form of a neutral/radical cation couple. For this purpose, we utilized the chemically synthesized and isolated radical cation salts of all EPT derivatives to examine the stability of the charged species. The thermal ellipsoid plots of isolated crystals of the radical cation salts are shown in Fig. S1 (ESI†). The isolation of X-ray quality crystals of radical cations confirms the substantial stability of charged forms, especially, 1,9-dimethylated strained phenothiazine derivatives. To further evaluate the chemical stability of radical cation forms in solution phase, we analyzed samples using UV-vis spectroscopy.

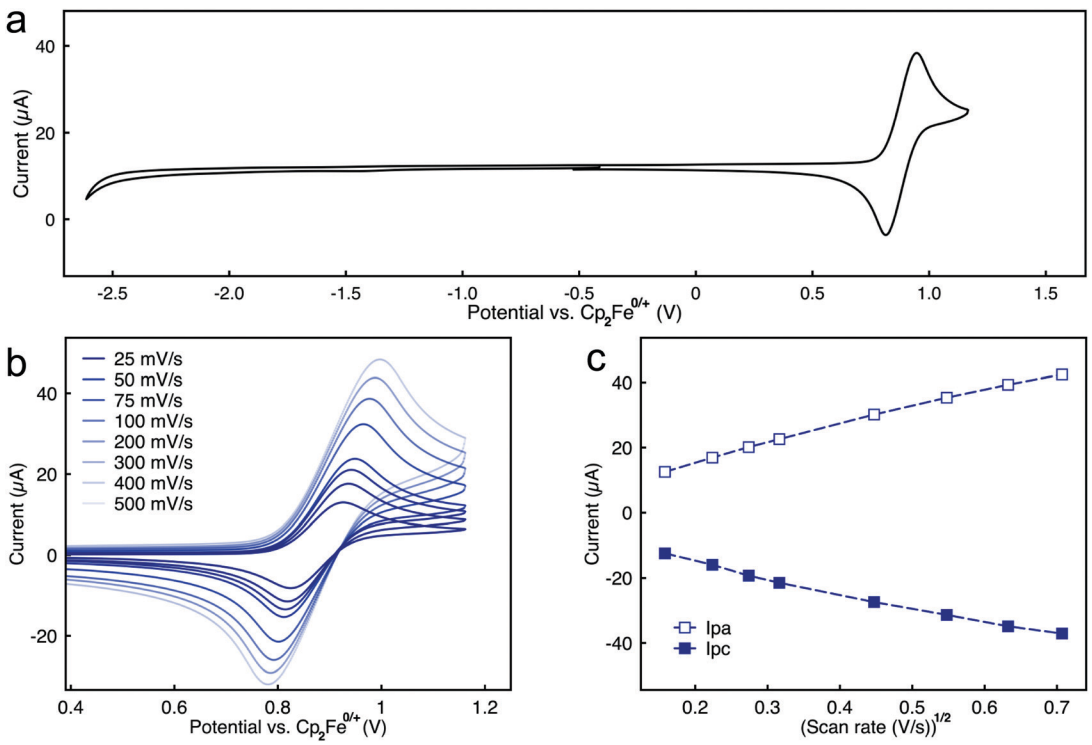

Fig. 4 Cyclic voltammogram of 1,9-DMe-3,7-BCF_3EPT at 1 mM in 0.1 M nBu_4NPF_6/DCM, recorded at a scan rate of 100 mV s^{-1} (a). The potential is calibrated to $Cp_2Fe^{0/+}$ at 0 V, using ferrocene as an internal reference. The scan-rate dependent cyclic voltammograms of the first oxidation event of 1,9-DMe-3,7-BCF_3EPT at 1 mM in 0.1 M nBu_4NPF_6 in DCM, recorded at scan rates ranging from 25 to 500 mV s^{-1} (b). Plot of peak current *vs.* the square root of the scan rate (c).

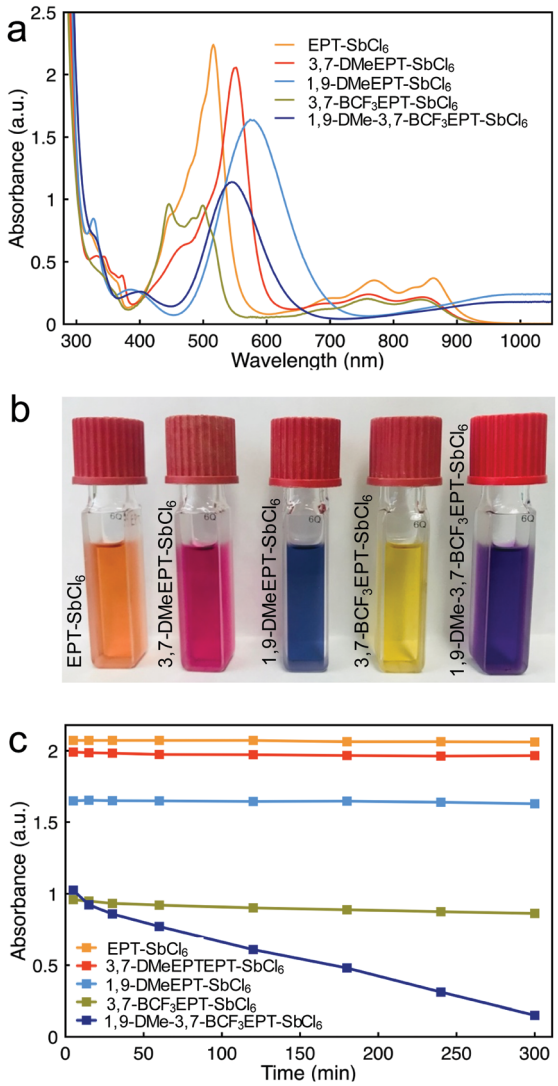

Fig. 5 UV-vis absorption spectra of EPT, 3,7-DMeEPT, 1,9-DMeEPT, 3,7-BCF_3EPT and 1,9-DMe-3,7-BCF_3EPT in their radical cation form at 0.20 mM (a), a photograph of cuvettes containing solutions of the radical cations dissolved in DCM and filled in 10 mm path length cuvettes (b), and a plot of absorbance *vs.* time for radical cations in DCM, collected at 5, 15, 30, 60, 120, 180, 240, and 300 min (c). The absorption intensity was monitored at absorption maxima of each radical cation (provided in Table S1, ESI†). The radical cation salts had hexachloroantimonate ($SbCl_6^-$) as the counter ion. UV-vis absorption spectra were recorded using 10 mm path length quartz cuvettes.

We began with a solution of radical cation salts in 0.2 mM concentration in anhydrous DCM using 10 mm path length cuvettes (Fig. 5). The absorption spectra of the neutral compounds (Fig. S6, ESI†) do not overlap with the regions of interest for the radical cations (Fig. 5a), where distinctive features are observed. In the neutral forms, the absorption spectra of the derivatives containing *ortho* substituents to N are blue shifted compared those that do not. Likewise, differences in the radical cation spectra are observed based on whether compounds contained *ortho* substituents. Specifically, the unstrained compounds exhibit features in close proximity and intensity in the region from 400–600 nm. However, the radical cations of strained 1,9-DMeEPT and 1,9-DMe-3,7-BCF_3EPT lack the finer structure in the lower energy region and instead show a broad absorption, and each exhibits a similarly shaped, more intense absorption feature between 500 and 600 nm that lacks the definition observed in the unstrained equivalents (Fig. 5a and Fig. S6, ESI†).

We monitored the shape and intensity changes of radical cation absorption spectra for 5 h after dissolving the isolated salts in anhydrous DCM at 0.2 mM (Fig. S7, ESI†). Plotted in Fig. 5c are the values for absorption intensity at maximum absorbance *vs.* time. For the unstrained derivatives as well as strained 1,9-DMeEPT, negligible loss in intensity was observed. However, for strained 1,9-DMe-3,7-BCF_3EPT, the intensity decreased by *ca.* two thirds over 5 h. Notably, in all cases, the shapes of the absorption spectra remained similar regardless of retention or loss in intensity (Fig. S7a–e, ESI†). We pondered the reason for the decay in absorbance intensity for 1,9-DMe-3,7-BCF_3EPT. No precipitate was observed in the cuvette, which led us to conclude that the compound was either being transformed into a new species *via* covalent bond cleavage/formation or underwent an electron-transfer reaction/self-discharge with the solvent and returned to its neutral form.

To determine whether the radical cation decomposed and/or underwent electron transfer more rapidly the low (0.2 mM) concentration employed due to trace impurities present in the solvent, we performed another UV-vis experiment at three elevated concentrations. Fig. 6a–c show the absorption spectra *vs.* time for three concentrations of radical cation form of 1,9-DMe-3,7-BCF_3EPT at 1, 5, and 10 mM in anhydrous DCM. We analyzed the radical cation salt at these elevated concentrations by using a shorter path length cuvette (2 mm) and by accepting that the absorption spectra of the 5 and 1 mM solution would saturate the detector at the most intense absorption region of radical cation (450–650 nm). Therefore, we monitored the absorption intensity changes in the low energy region (951 nm) for all concentrations. If it is true that trace impurities are responsible for an electron-transfer reaction that causes the radical cation of 1,9-DMe-3,7-BCF_3EPT to transform into its neutral form more rapidly at lower concentrations, and if impurities are acting as reagents rather than catalysts, then at a sufficiently high concentration, the rate of radical cation loss over time should be much lower.[39] As shown in Fig. 6d, radical cations decayed at a faster rate during the first hour compared to the remaining 4 hours, which might indicate that radical cations react with most of the trace solvent impurities just after dissolution. It appears that (Fig. 6d) radical cations are more persistent in the solution when moving from 1 mM to 10 mM concentration and the rate of decay is inversely proportional to the concentration. This result offers promise for higher stability and less material decomposition at elevated concentrations in solution phase, as we speculated.

As the radical cation form of 1,9-DMe-3,7-BCF_3EPT shows a significant chemical stability at a higher concentration (10 mM) in solution, we sought to analyze the radical cation stability in the solid state to evaluate this material as a stable chemical oxidant. In general, radical cations can be generated using a

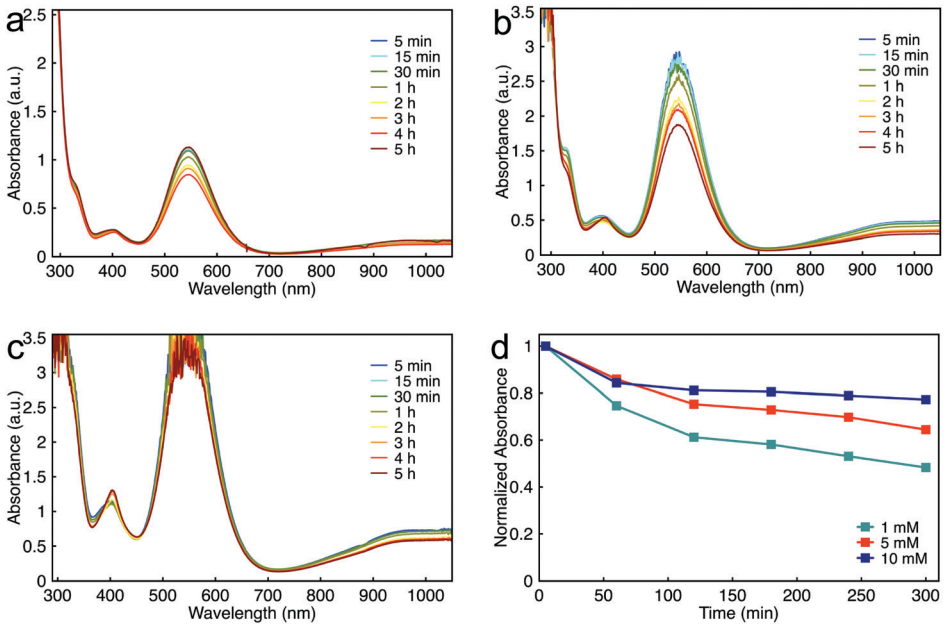

Fig. 6 UV-vis absorption spectra of 1,9-DMe-3,7-BCF$_3$EPT-SbCl$_6$ radical cation salts at 1 mM (a), 5 mM (b), 10 mM (c), in DCM, and a plot of normalized absorbance (at 951 nm) *vs.* time for radical cations at each concentration (d), collected at 5,15, 30, 60, 120, 180, 240, and 300 min. UV-vis absorption spectra were recorded using 2 mm path length quartz cuvettes.

few different techniques including bulk electrolysis, irradiation with gamma rays, and reaction with a chemical oxidant.[29,40,41] Of these methods, the use of chemical oxidants is quite simple. The chemical radical cation generation process is an electron transfer reaction where the oxidant accepts an electron from the neutral compound, thereby generating the radical cation

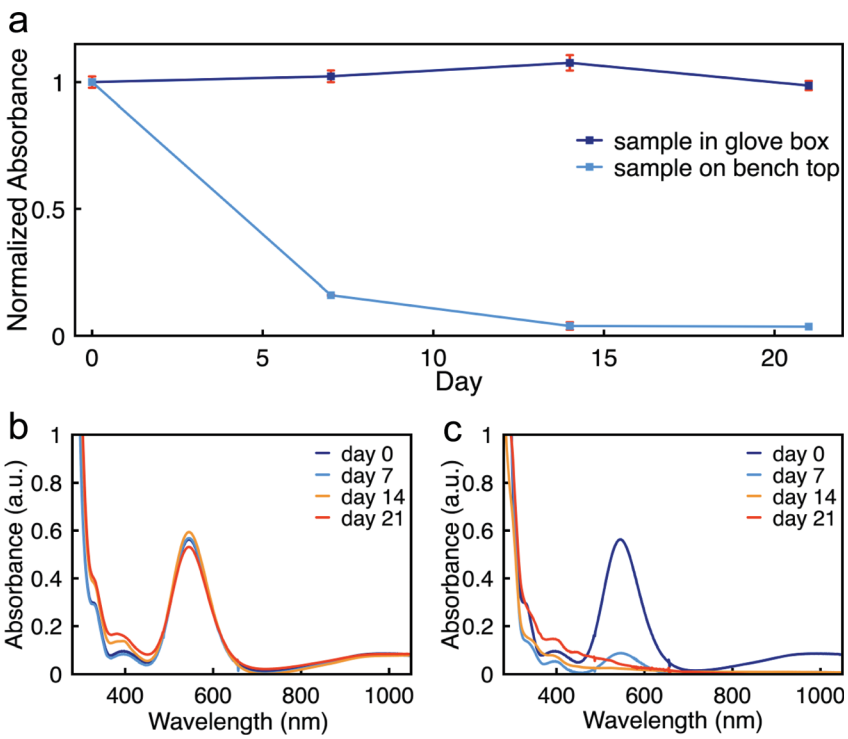

Fig. 7 Solid state stability of 1,9-DMe-3,7-BCF$_3$EPT-SbCl$_6$ on day 0, 7, 14, and 21 following storage in glass vials, placed in an argon filled glove box in light and on a bench top in light. Normalized absorbance intensity at 545 nm *vs.* time for 1,9-DMe-3,7-BCF$_3$EPT-SbCl$_6$ (a). UV-vis absorption spectra of 1,9-DMe-3,7-BCF$_3$EPT-SbCl$_6$, stored in an argon filled glove box (b), on the bench top (c) at 1 mM in DCM. UV-vis absorption spectra were recorded using 2 mm path length quartz cuvettes.

form. For a compound to serve as a chemical oxidant, it is necessary that the oxidation potential of neutral form of the chemical oxidant be higher than the neutral form of molecule to be oxidized. As 1,9-DMe-3,7-BCF_3EPT shows the highest oxidation potential ($E^{0/+}_{1/2}$ = 0.88 V *vs.* $Cp_2Fe^{0/+}$) among molecules in this study, its radical cation form should be able to chemically oxidize all phenothiazine derivatives, ranging from the lowest oxidation potential 3,7-DMeEPT ($E^{0/+}_{1/2}$ = 0.13 V *vs.* $Cp_2Fe^{0/+}$) to the next highest oxidation potential 3,7-BCF_3EPT ($E^{0/+}_{1/2}$ = 0.61 V *vs.* $Cp_2Fe^{0/+}$).

For this purpose, 1,9-DMe-3,7-BCF_3EPT-$SbCl_6$ was freshly synthesized and stored under two different conditions to examine its shelf life stability in the solid state for three weeks: (i) stored in a glass vial inside an argon filled glove box, and (ii) stored in a glass vial on the bench top. In addition to the radical cations of 1,9-DMe-3,7-BCF_3EPT, we analyzed the shelf life stability of freshly synthesized EPT-$SbCl_6$ as a control. As shown in Fig. 7 (1,9-DMe-3,7-BCF_3EPT-$SbCl_6$) and Fig. S8 (ESI†) (EPT-$SbCl_6$), the UV-vis spectra of radical cation samples were recorded on days 0, 7, 14, and 21 after freshly preparing radical cation solutions in anhydrous DCM. We analyzed 1,9-DMe-3,7-BCF_3EPT radical cation at 1 mM in 2 mm pathlength cuvettes.

EPT-$SbCl_6$ stored in the glove box and on the benchtop remained stable over three weeks without showing new peaks or without losing absorption intensity on UV-vis spectra (Fig. S8b and c, ESI†). The plot of normalized absorbance intensity at maximum absorbance *vs.* time of the EPT radical cation (Fig. S8a, ESI†) shows that it is stable in solid state for three weeks, regardless of the exclusion of water and oxygen or not. 1,9-DMe-3,7-BCF_3EPT-$SbCl_6$ showed environment-dependent stability. Although, the sample stored in the glove box remained similarly stable to EPT-$SbCl_6$ (Fig. 7a and b), the one kept on the benchtop decomposed significantly in the solid state (Fig. 7a and c). The loss of absorbance intensity is evident in the spectrum shown in Fig. 7c; the change in spectral shape indicates that 1,9-DMe-3,7-BCF_3EPT-$SbCl_6$ is sensitive to atmospheric moisture and/or air. However, its stability is greater than that of Magic Blue (MB, tris(4-bromophenylaminium)hexachloroantimonate), a commercially available chemical oxidant that has been employed as a one-electron oxidant in various fields,[42,43] is also known that to decompose in the solid state – even upon storage in an inert atmosphere, generating byproducts called the "blues brothers", by dimerizing through its labile C–Br bonds.[44,45] This not only prevents the accuracy of the quantitative analysis of the oxidation process, but also may mislead the spectroscopic analysis. However, 1,9-DMe-3,7-BCF_3EPT-$SbCl_6$ is at least as stable in an inert environment in the solid state, perhaps due to its strong covalent bonds. We suspect that 1,9-DMe-3,7-BCF_3EPT-$SbCl_6$ decomposed in ambient conditions due to the formation of S=O or SO_2 compounds by reacting with atmospheric oxygen/water.

Conclusions

Here we showed that the combination of electron-donating groups positioned at locations that prevent the relaxation of the radical cation form, in combination with electron-withdrawing groups at unstrained positions, have an additive effect on the oxidation potential of phenothiazines compared to derivatives having only one type of substituent. The oxidation potential of both strained and electron-withdrawing substituents resulted in the creation of a new high-potential redox couple with different electronic structure compared to its unstrained counterparts. The first oxidation event of the neutral compound is reversible by cyclic voltammetry at scan rates from 25 to 500 mV s^{-1}. Importantly, the introduction of substituents to create this high-potential couple did not bring the reduction event into the solvent window. This result highlights a key advantage of this approach over introduction of more electron-withdrawing groups to raise oxidation potentials, which – if sufficiently electron-withdrawing – bring the first reduction event, which is irreversible, into the solvent window. This feature may allow for strained phenothiazines to be used in applications that involve highly reducing environments and for their radical cation to be used as a strong oxidizing agent with stability greater that other organic oxidants.

Experimental section

I. General

Potassium trifluoroacetate, copper(I) iodide, and cesium fluoride were purchased from Sigma Aldrich. Sodium hydride (60% dispersion in mineral oil), magnesium sulfate, *N*-methylpyrrolidone (NMP), 1,3-dimethyl-2-imidazolidinone (DMI), sodium sulfite, potassium hydroxide and antimony pentachloride ($SbCl_5$) were purchased from Acros Organics. Bromine, acetic acid, and tetrabutylammonium hexafluorophosphate (nBu_4NPF_6) were purchased from Sigma Aldrich. Anhydrous dichloromethane (DCM), anhydrous tetrahydrofuran (THF), and anhydrous *N*,*N*-dimethylformamide (DMF) were purchased from VWR and stored in a solvent purification system (L.T. Technologies). Silica gel used for column chromatography was purchased from Sorbent Technologies. Ethyl acetate and hexanes for column chromatography were purchased from Avantor Performance Materials. Solvents used for NMR spectroscopy were obtained from Cambridge Isotope Laboratories. ^{1}H, ^{19}F and ^{13}C NMR spectra were obtained on a 400 MHz Varian NMR spectrometer. ^{19}F NMR, chemical shifts are reported *vs.* $CFCl_3$ at 0 ppm by adjusting the chemical shift of hexafluorobenzene (Alfa Aesar), used as an internal reference, to −164.9 ppm. Mass spectra were obtained on an Agilent 5973 Network mass selective detector attached to Agilent 6890N Network GC system. Elemental analyses were performed by Atlantic Microlab, Inc.

II. Synthesis

N-Ethylphenothiazine (EPT),[46] *N*-ethyl-3,7-dimethylphenothiazine (3,7-DMeEPT),[47] *N*-ethyl-3,7-bis(trifluoromethyl)phenothiazine (BCF_3EPT),[38] bis(*o*-tolyl)amine, 1,9-dimethylphenothiazine (1,9-DMePT), *N*-ethyl-1,9-dimethylphenothiazine (1,9-DMeEPT),[37] and *N*-ethylphenothiazine-hexachloroantimonate (EPT-$SbCl_6$),[29] were synthesized as previously reported.

3,7-Dibromo-1,9-dimethylphenothiazine (1,9-DMe-3,7-DBrPT). In an oven-dried 250 mL round-bottomed flask under nitrogen atmosphere, 1,9-DMePT (3.25 g, 14.3 mmol) was dissolved in anhydrous acetic acid (100 mL). A solution of bromine (2.12 mL, 41.5 mmol) in acetic acid (15 mL) was slowly transferred into the reaction mixture using an addition funnel. Then the reaction mixture was stirred in room temperature for a day until consumption of starting materials. Sodium sulfite (1.22 g, 2.02 mmol) was added into reaction mixture and stirred for 2 h till get a gray solution. After that reaction mixture was transferred into a 1 L beaker. Potassium hydroxide (2.51 g, 42.9 mmol) was dissolved in deionized water (100 mL) and the volume was raised to 300 mL after adding ice. This solution was poured into the reaction mixture and stirred using a glass rod, yielding a gray precipitate, which was filtered, rinsed with more deionized water, then dried overnight in a vacuum oven (50 °C, −0.1 MPa). Finally, the solid product was crystallized from ethanol, yielding the product as a gray crystalline solid (2.78 g, 51%). ^{1}H NMR (400 MHz, DMSO-d_6) δ 7.18 (m, 2H), 7.09 (m, 2H), 6.85 (s, 1H), 2.25 (s, 6H). ^{13}C NMR (100 MHz, $CDCl_3$) δ 138.9, 133.3, 133.0, 131.7, 127.2, 114.3, 16.8. GCMS: *m*/*z* 385 (100%), 383 (91%), 304 (37%), 302 (34%), 224 (38%), 192 (12%), 180 (8%), 111(10%). Anal. calcd for $C_{14}H_{11}Br_2NS$: C, 43.66; H, 2.88; N, 3.64. Found C, 43.85; H, 2.97; N, 3.63.

3,7-Dibromo-*N*-ethyl-1,9-dimethylphenothiazine (1,9-DMe-3,7-DBrEPT). In an oven-dried 250 mL round-bottomed flask under nitrogen atmosphere, 1,9-DMe-3,7-DBrPT (3.00 g, 7.80 mmol) was dissolved in a solution of anhydrous DMF (60 mL) and anhydrous THF (60 mL). Sodium hydride (0.78 g, 60 wt% in mineral oil, 20 mmol) was added at room temperature, and the reaction mixture was stirred for 30 min. After that bromoethane (1.02 g, 48.6 mmol) was added to the reaction mixture and round bottom flask was equipped with a reflux condenser. Then the reaction mixture was refluxed by heating in an oil bath at 90 °C for 12 h. After completion the reaction, reaction mixture was cooled to room temperature and quenched with water. The organic product was extracted with ethyl acetate, and it was washed with brine and dried over $MgSO_4$. The organic extracts were filtered and concentrated by rotary evaporation. The resulting organic crude was purified by silica gel column chromatography using a gradient of 0–4% ethyl acetate in hexanes as eluent, yielding the product as a white solid (2.15 g, 66%). ^{1}H NMR (400 MHz, DMSO-d_6) δ 7.41–7.31 (m, 4H), 3.39 (q, J = 7.0, 2H), 2.34 (s, 6H), 0.95 (t, J = 7.1, 3H). ^{13}C NMR (100 MHz, $CDCl_3$) δ 142.9, 135.9, 135.8, 132.2, 127.1, 117.4, 49.6, 18.2, 14.1. GCMS: *m*/*z* 413 (23%), 384 (100%), 382(54%), 304 (8%), 223 (10%). Anal. calcd for $C_{16}H_{15}Br_2NS$: C, 46.51; H, 3.66; N, 3.39. Found C, 46.59; H, 3.82; N, 3.34.

***N*-Ethyl-1,9-dimethyl-3,7-bis(trifluoromethyl)phenothiazine (1,9-DMe-3,7-BCF$_3$EPT).** 1,9-DMe-3,7-DBrEPT (1.25 g, 3.03 mmol) and copper(I) iodide (4.61 g, 24.2 mmol) were added into an oven dried 100 mL pressure vessel under nitrogen atmosphere. The pressure vessel was transferred to an argon filled glove box, then potassium trifluoroacetate (2.76 g, 18.2 mmol) and cesium fluoride (0.99 g 6.5 mmol) were added into the pressure vessel and removed from the glove box. *N*-Methylpyrrolidinone (NMP) (44 mL) and 1,3-dimethyl-2-imidazolidinone (10 mL) were added under N_2 atmosphere to the reaction mixture, which was sparged with N_2 for 10 min while immersed in oil bath preheated to 90 °C. The pressure vessel was sealed, and the temperature of the oil bath was raised to 180 °C after which the reaction mixture was stirred for 48 h. The reaction flask was removed from the oil bath, and the reaction mixture was allowed to cool to room temperature, then diluted with ethyl acetate and filtered through a pad of Celite. Water was added to the filtrate and organic product was extracted with ethyl acetate. The combined organic layers were washed with brine and dried over $MgSO_4$. The organic extracts were filtered and concentrated by rotary evaporation. The resulting organic crude was purified by silica gel column chromatography using a gradient of 0–2% ethyl acetate in hexanes as the eluent, yielding the product as a white crystalline solid (0.62 g, 48%). ^{1}H NMR (400 MHz, DMSO-d_6) δ 7.58 – 7.51 (m, 4H), 3.57 (q, J = 7.1 Hz, 2H), 2.43 (s, 6H), 0.99 (t, J = 7.1 Hz, 3H). ^{13}C NMR (100 MHz, $CDCl_3$) δ 147.1, 134.9, 134.5, 127.0, 125.5, 122.8, 122.1, 50.1, 18.9, 14.8. ^{19}F NMR (400 MHz, $CDCl_3$) δ −65.4 (s, 6F). GCMS: *m*/*z* 391 (23%), 362 (100%), 330 (8%). Anal. calcd for $C_{18}H_{15}F_6NS$: C, 55.24; H, 3.86; N, 3.58. Found C, 55.04; H, 4.05; N, 3.60.

***N*-Ethyl-3,7-dimethylphenothiazine hexachloroantimonate (3,7-DMeEPT-SbCl$_6$).** 3,7-DMeEPT (0.10 g, 0.39 mmol) was dissolved in anhydrous dichloromethane (5 mL) in an oven-dried 25 mL round-bottomed flask fitted with a rubber septum under nitrogen atmosphere after which the round-bottomed flask immersed in an ice water bath for 10 min. Then antimony pentachloride (0.080 mL, 0.58 mmol) was added into reaction mixture and stirred 15 min. Upon completion of the reaction, anhydrous diethyl ether (15 mL) was added gradually with continued stirring, resulting in a dark pink precipitate. The precipitate was filtered under nitrogen, then washed with more diethyl ether (20–30 mL) to remove unreacted starting material. The solid dark pink product (0.11 g, 50%) was dried under nitrogen and stored in a glove box. To grow crystals of this product, a saturated solution of 3,7-DMeEPT-SbCl$_6$ salt in anhydrous DCM was prepared. Then, a small volume of saturated solution (0.5 mL) transferred in an NMR tube and slowly layered it with anhydrous toluene (0.5 mL) to form two layers. Finally, the NMR tube was capped and vertically placed in a freezer set at 4 °C, and crystals formed at the interface of the solvents.

***N*-Ethyl-1,9-dimethylphenothiazine hexachloroantimonate (1,9-DMeEPT-SbCl$_6$).** 1,9-DMeEPT (0.10 g, 0.39 mmol) was dissolved in anhydrous dichloromethane (5 mL) in an oven-dried 25 mL round-bottomed flask fitted with a rubber septum under nitrogen atmosphere, then round-bottomed flask was cooled in an ice water bath for 10 minutes. Then antimony pentachloride (0.080 mL, 0.58 mmol) was added into reaction mixture and stirred 15 minutes. Upon completion of the reaction, anhydrous diethyl ether (15 mL) was added gradually with continued stirring, resulting in a blue precipitate. The precipitate was filtered under nitrogen, then washed with more diethyl ether (20–30 mL) to remove unreacted starting material. The solid blue product (0.10 g, 43%) was dried under nitrogen and stored in a glove box. To grow crystals of this product, a saturated

solution of 1,9-DMeEPT-$SbCl_6$ salt in anhydrous DCM was prepared. Then, a small volume of saturated solution (0.5 mL) transferred in an NMR tube and slowly layered it with anhydrous diethyl ether (0.5 mL) to form two layers. Finally, the NMR tube was capped and vertically placed in a freezer set at 4 °C, and crystals formed at the interface of the solvents.

***N*-Ethyl-3,7-bis(trifluoromethyl)phenothiazine hexachloroantimonate (3,7-BCF_3EPT-$SbCl_6$).** 3,7-BCF_3EPT (0.10 g, 0.28 mmol) was dissolved in anhydrous dichloromethane (5 mL) in an oven-dried 25 mL round-bottomed flask fitted with a rubber septum under nitrogen atmosphere, then round-bottomed flask was cooled in an ice water bath for 10 minutes. Antimony pentachloride (0.050 mL, 0.41 mmol) was added into reaction mixture and stirred 15 minutes. Upon completion of the reaction, anhydrous diethyl ether (15 mL) was added gradually with continued stirring, resulting in a dark green precipitate. The precipitate was filtered under nitrogen, then washed with more diethyl ether (20–30 mL) to remove unreacted starting material. The solid dark green product (0.12 g, 66%) was dried under nitrogen and stored in a glove box.

***N*-Ethyl-1,9-dimethyl-3,7-bis(trifluoromethyl)phenothiazine hexachloroantimonate (1,9-DMe-3,7-BCF_3EPT-$SbCl_6$)**

1,9-DMe-3,7-BCF_3EPT (0.18 g, 0.37 mmol) was dissolved in anhydrous dichloromethane (5 mL) in an oven-dried 25 mL round-bottomed flask fitted with a rubber septum under nitrogen atmosphere, then round-bottomed flask was cooled in an ice water bath for 10 minutes. Antimony pentachloride (0.080 mL, 0.55 mmol) was added into reaction mixture and stirred 15 minutes. Upon completion of the reaction, anhydrous diethyl ether (15 mL) was added gradually with continued stirring, resulting in a blue precipitate. The precipitate was filtered under nitrogen, then washed with more diethyl ether (20–30 mL) to remove unreacted starting material. The solid purple product (0.14 g, 42%) was dried under nitrogen and stored in a glove box. To grow crystals of this product, a saturated solution of 1,9-DMe-3,7-BCF_3EPT-$SbCl_6$ salt in anhydrous DCM was prepared. Then, a small volume of saturated solution (0.5 mL) transferred in an NMR tube and slowly layered it with anhydrous diethyl ether (0.5 mL) to form two layers. Finally, the NMR tube was capped and vertically placed in a freezer set at 4 °C, and crystals formed at the interface of the solvents.

III. X-ray crystallography

X-ray diffraction data were collected either at 90.0(2) K at 180(1) K on a Bruker D8 Venture kappa-axis diffractometer using MoK(alpha) X-rays. Raw data were integrated, scaled, merged and corrected for Lorentz-polarization effects using the APEX3 package.[48] Corrections for absorption were applied using SADABS.[49] The structure was solved by direct methods (SHELXT)[50] and refinement was carried out against F^2 by weighted full-matrix least-squares (SHELXL).[51] Hydrogen atoms were found in difference maps, but subsequently placed at calculated positions and refined using a riding model. Non-hydrogen atoms were refined with anisotropic displacement parameters. Atomic scattering factors were taken from the International Tables for Crystallography.[52]

IV. Computational studies

All density functional theory (DFT) calculations were performed using the Gaussian09 (Revision A.02b) software suite. Geometry optimizations of the neutral and radical-cation states were carried out using the B3LYP functional at the 6-311G(d,p) level of theory.[53] Frequency analyses of all (fully relaxed) optimized geometries were performed to ensure that the geometries were energetic minima. AIP of EPT, 3,7-DMeEPT, 1,9-DMeEPT, and 3,7-BCF_3EPT was taken from ref. 37.

V. Electrochemical analysis

Cyclic voltammetry (CV) experiments were performed with a CH Instruments 600D potentiostat using a three-electrode system with glassy carbon as the working electrode, freshly anodized Ag/AgCl as the reference electrode, and a Pt wire as the counter electrode at 1 mM analyte in 0.1 M nBu$_4$NPF$_6$ in DCM. Voltammograms were recorded at a scan rate of 100 mV s^{-1}. Ferrocene or decamethylferrocene was used as an internal reference and oxidation potentials were calibrated relative to ferrocenium/ferrocene ($Cp_2Fe^{+/0}$). The diffusion coefficients of the active species at 1 mM concentration were calculated using Randles–Sevcik equation,[54]

$$i_p = 0.4463nFAc\left(\frac{nFD}{RT}\nu\right)^{0.5}$$

where i_p is the peak current (A), n is the number of electrons transferred (−), F is the Faraday constant (96 485 C mol^{-1}), A is the electrode area (cm^2), c is the concentration (mol cm^{-3}), D is the diffusion coefficient (cm^2 s^{-1}), R is the gas constant (8.314 J mol^{-1} K^{-1}), T is the absolute temperature (K), and ν is the scan rate (V s^{-1}). The following scan rates were used for diffusion coefficient calculations: 25, 50, 75, 100, 200, 300, 400, and 500 mV s^{-1}.

VI. UV-vis spectroscopy

UV-vis spectra were obtained using optical glass cuvettes (Starna) with 2 or 10 mm path length on an Agilent 8453 diode array spectrophotometer. All the radical cation solutions were prepared in anhydrous DCM and transferred into cuvettes inside an argon filled glovebox. The capped cuvettes were taken out from the glove box for spectral analysis.

UV-vis study at 0.2 mM concentration. All phenothiazine radical cation salts (EPT-$SbCl_6$, 3,7-DMeEPT-$SbCl_6$, 1,9-DMeEPT-$SbCl_6$, 3,7-BCF_3EPT-$SbCl_6$, and 1,9-DMe-3,7-BCF_3EPT-$SbCl_6$) were dissolved in anhydrous DCM at 0.2 M and pipetted to 1 cm path length cuvettes. UV-vis spectra were collected at 5, 15, 30, 60, 120, 180, 240, 300 min after preparing samples.

UV-vis study at different concentrations. 1,9-DMe-3,7-BCF_3EPT-$SbCl_6$ was dissolved in anhydrous DCM at 1, 5, and 10 mM and pipetted to 2 mm path length cuvettes. UV-vis spectra were collected at 5, 15, 30, 60, 120, 180, 240, 300 min after preparing samples.

UV-vis study for shelf stability. Freshly synthesized radical cation salts of EPT-$SbCl_6$ and 1,9-DMe-3,7-BCF_3EPT-$SbCl_6$ were stored in two different environments; 1. stored in a glass vial and placed inside an argon filled glove box, 2. stored in a glass vial and placed on the bench top. The radical cation salts were weighed either inside of the glove box or outside of the glove box to prepare samples for UV-vis analysis, depending on where it has been stored. Then, all solutions were prepared in anhydrous DCM and transferred into cuvettes inside an argon filled glovebox. EPT-$SbCl_6$ was analyzed at 0.2 mM (in 10 mm pathlength cuvette) as its solubility is less than 1 mM in DCM and 1,9-DMe-3,7-BCF_3EPT-$SbCl_6$ was analyzed at 1 mM (in 2 mm pathlength cuvette) as it highly decays at 0.2 mM. At days 0, 7, 14 and 21, required amounts (to make a 0.2 or 1 mM solution) of each radical cation salt stored on bench-top (weighed outside the glovebox) and the ones stored inside the box (weighed inside the glovebox) were dissolved in anhydrous DCM (inside the glovebox) and prepared UV-vis samples for analysis.

Conflicts of interest

There are no conflicts to declare.

Acknowledgements

This work was funded by the National Science Foundation's Division of Chemistry (Award 1300653) and EPSCoR Program (Award 1355438). We thank Corrine Elliott and Chad Risko for their computational chemistry efforts. While their results are cited, we could not have done this work without them.

References

1 S. Ergun, C. F. Elliott, A. P. Kaur, S. R. Parkin and S. A. Odom, Overcharge Performance of 3,7-disubstituted *N*-Ethylphenothiazine Derivatives in Lithium-ion Batteries, *Chem. Commun.*, 2014, **50**, 5339–5341.

2 J. Zhang, J. Huang, L. A. Robertson, I. A. Shkrob and L. Zhang, Comparing Calendar and Cycle Life Stability of Redox Active Organic Molecules for Nonaqueous Redox Flow Batteries, *J. Power Sources*, 2018, **397**, 214–222.

3 L. P. Hammett, The Effect of Structure Upon the Reactions of Organic Compounds. Benzene Derivatives, *J. Am. Chem. Soc.*, 1937, **59**, 96–103.

4 M. J. Dewar and P. J. Grisdale, Substituent Effects. I. Introduction, *J. Am. Chem. Soc.*, 1962, **84**, 3539–3541.

5 J. A. Kowalski, T. J. Carney, J. Huang, L. Zhang and F. R. Brushett, An investigation on the impact of halidization on substituted dimethoxybenzenes, *Electrochim. Acta*, 2020, **335**, 135580.

6 Z. Zhang, L. Zhang, J. A. Schlueter, P. C. Redfern, L. Curtiss and K. Amine, Understanding the Redox Shuttle Stability of 3,5-di-*tert*-butyl-1, 2-dimethoxybenzene for Overcharge Protection of Lithium-ion Batteries, *J. Power Sources*, 2010, **195**, 4957–4962.

7 J. Huang, L. Su, J. A. Kowalski, J. L. Barton, M. Ferrandon, A. K. Burrell, F. R. Brushett and L. Zhang, A Subtractive Approach to Molecular Engineering of Dimethoxybenzene-Based Redox Materials for Non-aqueous Flow Batteries, *J. Mater. Chem. A*, 2015, **3**, 14971–14976.

8 P. Schwager, H. Bülter, I. Plettenberg and G. Wittstock, Review of Local In Situ Probing Techniques for the Interfaces of Lithium-Ion and Lithium–Oxygen Batteries, *Energy Technol.*, 2016, **4**, 1472–1485.

9 L. Moshurchak, C. Buhrmester, R. Wang and J. Dahn, Comparative Studies of Three Redox Shuttle Molecule Classes for Overcharge Protection of LiFePO4-Based Li-ion Cells, *Electrochim. Acta*, 2007, **52**, 3779–3784.

10 X. Wei, W. Xu, M. Vijayakumar, L. Cosimbescu, T. Liu, V. Sprenkle and W. Wang, TEMPO-Based Catholyte for High-Energy Density Nonaqueous Redox Flow Batteries, *Adv. Mater.*, 2014, **26**, 7649–7653.

11 B. J. Bergner, A. Schürmann, K. Peppler, A. Garsuch and J. r. Janek, TEMPO: A Mobile Catalyst for Rechargeable Li–O_2 Batteries, *J. Am. Chem. Soc.*, 2014, **136**, 15054–15064.

12 N. H. Attanayake, J. A. Kowalski, K. V. Greco, M. D. Casselman, J. D. Milshtein, S. J. Chapman, S. R. Parkin, F. R. Brushett and S. A. Odom, Tailoring Two-Electron-Donating Phenothiazines To Enable High-Concentration Redox Electrolytes for Use in Nonaqueous Redox Flow Batteries, *Chem. Mater.*, 2019, **31**, 4353–4363.

13 A. P. Kaur, S. Ergun, C. F. Elliott and S. A. Odom, 3,7-Bis-(trifluoromethyl)-*N*-ethylphenothiazine: A Redox Shuttle with Extensive Overcharge Protection in Lithium-ion Batteries, *J. Mater. Chem. A*, 2014, **2**, 18190–18193.

14 J. D. Milshtein, A. P. Kaur, M. D. Casselman, J. A. Kowalski, S. Modekrutti, P. L. Zhang, N. H. Attanayake, C. F. Elliott, S. R. Parkin, C. Risko, F. R. Brushett and S. A. Odom, High Current Density, Long Duration Cycling of Soluble Organic Active Species for Non-Aqueous Redox Flow Batteries, *Energy Environ. Sci.*, 2016, **9**, 3531–3543.

15 S. Li, X. Ai, H. Yang, Y. Cao and A. Polytriphenylamine-Modified, Separator with Reversible Overcharge Protection for 3.6 V-Class Lithium-ion Battery, *J. Power Sources*, 2009, **189**, 771–774.

16 V. Pasala, C. Ramachandra, S. Sethuraman, K. Ramanujam and A. High, Voltage Organic Redox Flow Battery with Redox Couples O2/Tetrabutylammonium Complex and Tris (4-bromophenyl) amine as Redox Active Species, *J. Electrochem. Soc.*, 2018, **165**, A2696–A2702.

17 R. P. Dunn, J. Kafle, F. C. Krause, C. Hwang, B. V. Ratnakumar, M. C. Smart and B. L. Lucht, Electrochemical Analysis of Li-ion Cells Containing Triphenyl Phosphate, *J. Electrochem. Soc.*, 2012, **159**, A2100–A2108.

18 M. D. Casselman, A. P. Kaur, K. A. Narayana, C. F. Elliott, C. Risko and S. A. Odom, The Fate of Phenothiazine-based Redox Shuttles in Lithium-ion Batteries, *Phys. Chem. Chem. Phys.*, 2015, **17**, 6905–6912.

19 Z. Chen and K. Amine, Bifunctional Electrolyte Additive for Lithium-ion Batteries, *Electrochem. Commun.*, 2007, **9**, 703–707.

20 L. Zhang, Z. Zhang, H. Wu and K. Amine, Novel Redox Shuttle Additive for High-Voltage Cathode Materials, *Energy Environ. Sci.*, 2011, **4**, 2858–2862.
21 L. Moshurchak, W. Lamanna, M. Bulinski, R. Wang, R. R. Garsuch, J. Jiang, D. Magnuson, M. Triemert and J. Dahn, High-Potential Redox Shuttle for Use in Lithium-ion Batteries, *J. Electrochem. Soc.*, 2009, **156**, A309–A312.
22 F. Bell, A. Ledwith and D. Sherrington, Cation-Radicals: tris-(p-Bromophenyl) Amminium perchlorate and hexachloroatimonate, *J. Chem. Soc. C*, 1969, 2719–2720.
23 E. Steckhan, Indirect Electroorganic Syntheses—A Modern Chapter of Organic Electrochemistry [New Synthetic Methods (59)], *Angew. Chem., Int. Ed. Engl.*, 1986, **25**, 683–701.
24 N. A. Romero and D. A. Nicewicz, Organic photoredox catalysis, *Chem. Rev.*, 2016, **116**, 10075–10166.
25 J. A. Christensen, B. T. Phelan, S. Chaudhuri, A. Acharya, V. S. Batista and M. R. Wasielewski, Phenothiazine radical cation excited states as super-oxidants for energy-demanding reactions, *J. Am. Chem. Soc.*, 2018, **140**, 5290–5299.
26 D. T. Breslin and M. A. Fox, Excited-state behavior of thermally stable radical ions, *J. Phys. Chem.*, 1994, **98**, 408–411.
27 J. Grilj, E. N. Laricheva, M. Olivucci and E. Vauthey, Fluorescence of radical ions in liquid solution: wurster's blue as a case study, *Angew. Chem., Int. Ed.*, 2011, **50**, 4496–4498.
28 S. Green and M. A. Fox, Intramolecular photoinduced electron transfer from nitroxyl radicals, *J. Phys. Chem.*, 1995, **99**, 14752–14757.
29 S. A. Odom, S. Ergun, P. P. Poudel, S. R. Parkin and A. Fast, Inexpensive Method for Predicting Overcharge Performance in Lithium-ion Batteries, *Energy Environ. Sci.*, 2014, **7**, 760–767.
30 Z. Mi, P. Yang, R. Wang, J. Unruangsri, W. Yang, C. Wang and J. Guo, Stable Radical Cation-Containing Covalent Organic Frameworks Exhibiting Remarkable Structure-Enhanced Photothermal Conversion, *J. Am. Chem. Soc.*, 2019, **141**, 14433–14442.
31 N. Fukui, W. Cha, D. Shimizu, J. Oh, K. Furukawa, H. Yorimitsu, D. Kim and A. Osuka, Highly planar diarylamine-fused porphyrins and their remarkably stable radical cations, *Chem. Sci.*, 2017, **8**, 189–199.
32 J. Maier and D. Turner, Steric Inhibition of Resonance Studied by Molecular Photoelectron Spectroscopy. Part 1.—Biphenyls, *Faraday Discuss. Chem. Soc.*, 1972, **54**, 149–167.
33 L. Andrews, R. T. Arlinghaus and C. K. Payne, Absorption Spectra of Substituted Biphenyl and Related Cations in Solid Argon and a Comparison with Photoelectron Spectra, *J. Chem. Soc., Faraday Trans. 2*, 1983, 885–895.
34 G. R. Hutchison, M. A. Ratner and T. J. Marks, Hopping Transport in Conductive Heterocyclic Oligomers: Reorganization Energies and Substituent Effects, *J. Am. Chem. Soc.*, 2005, **127**, 2339–2350.
35 S. S. Zade and M. Bendikov, Twisting of Conjugated Oligomers and Polymers: Case Study of Oligo-and Polythiophene, *Chem. – Eur. J.*, 2007, **13**, 3688–3700.
36 R. A. Pascal, Twisted acenes, *Chem. Rev.*, 2006, **106**, 4809–4819.
37 M. D. Casselman, C. F. Elliott, S. Modekrutti, P. L. Zhang, S. R. Parkin, C. Risko and S. A. Odom, Beyond the Hammett Effect: Using Strain to Alter the Landscape of Electrochemical Potentials, *ChemPhysChem*, 2017, **18**, 2142–2146.
38 S. Ergun, M. D. Casselman, A. P. Kaur, N. H. Attanayake, S. R. Parkin and S. A. Odom, Improved Synthesis of *N*-Ethyl-3, 7-Bis(Trifluoromethy) Phenothiazine, *New J. Chem.*, 2020, **44**, 11349–11355.
39 A. P. Kaur, O. C. Harris, N. H. Attanayake, Z. Liang, S. R. Parkin, M. H. Tang and S. A. Odom, Quantifying Environmental Effects on the Solution and Solid-State Stability of a Phenothiazine Radical Cation, *Chem. Mater.*, 2020, **32**, 3007–3017.
40 H. D. Roth, Structure and Reactivity of Organic Radical Cations. *In Photoinduced Electron Transfer IV*, Springer, 1992.
41 M. Schmittel and A. Burghart, Understanding Reactivity Patterns of Radical Cations, *Angew. Chem., Int. Ed. Engl.*, 1997, **36**, 2550–2589.
42 N. G. Connelly and W. E. Geiger, Chemical Redox Agents for Organometallic Chemistry, *Chem. Rev.*, 1996, **96**, 877–910.
43 M. R. Talipov and R. Rathore, *Robust Aromatic Cation Radicals as Redox Tunable Oxidants. Organic Redox Systems: Synthesis, Properties, and Applications*, 2015.
44 M. R. Talipov, M. M. Hossain, A. Boddeda, K. Thakur and R. A. Rathore, Search for Blues Brothers: X-ray Crystallographic/Spectroscopic Characterization of the Tetraarylbenzidine Cation Radical as a Product of Aging of Solid Magic Blue, *Org. Biomol. Chem.*, 2016, **14**, 2961–2968.
45 L. Eberson and B. Larsson, Electron Transfer Reactions in Organic Chemistry. IX.* Acyloxylation and/or Debromodimerization Instead of, *Acta Chem. Scand.*, 1986, **40**, 210–225.
46 K. A. Narayana, M. D. Casselman, C. F. Elliott, S. Ergun, S. R. Parkin, C. Risko and S. A. Odom, *N*-Substituted Phenothiazine Derivatives: How the Stability of the Neutral and Radical Cation Forms Affects Overcharge Performance in Lithium-ion Batteries, *ChemPhysChem*, 2015, **16**, 1179–1189.
47 S. Ergun, C. F. Elliott, A. P. Kaur, S. R. Parkin and S. A. Odom, Controlling Oxidation Potentials in Redox Shuttle Candidates for Lithium-ion Batteries, *J. Phys. Chem. C*, 2014, **118**(27), 14824–14832.
48 *Bruker-AXS*, APEX3 Bruker-AXS Inc., Madison, WI, USA, 2016.
49 L. Krause, R. Herbst-Irmer, G. M. Sheldrick and D. Stalke, Comparison of Silver and Molybdenum Microfocus X-ray Sources for Single-Crystal Structure Determination, *J. Appl. Crystallogr.*, 2015, **48**, 3–10.
50 G. M. Sheldrick, SHELXT-Integrated Space-Group and Crystal-Structure Determination, *Acta Crystallogr., Sect. A: Found. Adv.*, 2015, **71**, 3–8.
51 G. M. Sheldrick, Crystal Structure Refinement with SHELXL, *Acta Crystallogr., Sect. C: Struct. Chem.*, 2015, **71**, 3–8.
52 International Tables for Crystallography, *vol C: Mathematical, Physical and Chemical Tables*, ed. A. J. C. Wilson, Kluwer Academic Publishers, Holland, 1992.
53 M. Frisch; G. Trucks; H. Schlegel; G. Scuseria; M. Robb; J. Cheeseman; G. Scalmani; V. Barone; B. Mennucci and G. Petersson, *Gaussian 09*, Gaussian, Inc, 2009, **32**, 5648–5652.
54 R. G. Compton and C. E. Banks, *Understanding Voltammetry*, Imperial College Press, London, 2nd edn, 2011.